Journal of Marine Research, 53, 79–106, 1995

A decadal oscillation due to the coupling between an ocean circulation model and a thermodynamic sea-ice model

by Sheng Zhang[1,2], Charles A. Lin[1] and Richard J. Greatbatch[2]

ABSTRACT

A 3-dimensional, planetary-geostrophic, ocean general circulation model is coupled to a thermodynamic sea-ice model. The thermal coupling takes account of the insulating effect of the ice. A simple approach is taken in the case of the freshwater flux by allowing this to pass through the ice, except that some is used for snow accumulation. It is then modified by salinity rejection/dilution due to freezing/melting. The model has idealized box geometry extending 60° in both latitude and longitude, with a horizontal resolution of 2° and 14 vertical levels. Annual mean surface forcings are used. The coupled system is first spun up using restoring conditions on both surface temperature and surface salinity to reach a steady state which includes ice in the high latitudes. A switch of the surface forcing to mixed boundary conditions (restoring on temperature and flux on salinity) leads to an oscillation of period 17 years in the magnitude of the thermohaline circulation and the ice extent. The oscillation is due to a feedback between ice cover and ocean temperature. Since ice forms only in regions where the ocean loses heat to the atmosphere, the thermal insulation of an increased ice cover makes the ocean warmer. The thermohaline circulation plays a role in transporting this heat polewards, which in turn melts the ice. The heat loss over open water at high latitudes then leads to ice formation and the process repeats itself. Salinity rejection/dilution associated with ice formation/melting is shown to be of secondary importance in this oscillation. Rather, changes in surface salinity are dominated by changes in deep convection and the associated vertical mixing, which are themselves associated with the reduction in surface heat loss due to the insulating effect of the ice. As a consequence the model exhibits the negative correlation between surface salinity and ice extent that is observed in the high latitude North Atlantic.

1. Introduction

The ocean plays an important role in the earth's climate (e.g. Mysak and Lin, 1990; Weaver and Hughes, 1992). Its heat capacity is three orders of magnitude larger than that of the atmosphere; indeed, the top several meters of the world's oceans have the same heat capacity as that of the atmosphere. In addition, about half of the heat transport from low to high latitudes, required to maintain the current climate, is by the oceans. Thus the stability and variability of the thermohaline circulation, which is

1. Department of Atmospheric and Oceanic Sciences, and Centre for Climate and Global Change Research, McGill University, Montreal, Quebec, Canada, H3A 2K6.
2. Department of Physics, Memorial University of Newfoundland, St. John's, Newfoundland, Canada, A1B 3X7.

an important mechanism for the storage and transport of heat, is a subject of much current interest and research (Weaver and Hughes, 1992).

Bjerknes (1964) was the first to suggest that variations in the thermohaline circulation play a role in determining the interdecadal variability of sea surface temperature (SST) in the North Atlantic. This has been discussed further by Bryan and Stouffer (1991) and Gordon *et al.* (1992). Evidence for the role of the ocean has also been presented by Kushnir (1994), and Deser and Blackmon (1993). The latter have pointed out a relationship between variations in ice extent in the Labrador Sea and SST to the east of Newfoundland, with greater than normal ice extent preceeding lower than normal SST by about two years. Mysak *et al.* (1990) have suggested a mechanism for driving an interdecadal oscillation involving changes in precipitation, river run-off, Arctic sea ice, deep convection and Arctic cyclogenesis (see also Mysak and Power, 1992). They have linked their mechanism to the occurrence of the Great Salinity Anomaly in the late 1960's and early 1970's (Dickson *et al.,* 1988).

Starting from F. Bryan (1986a,b), various studies have used mixed boundary conditions to drive ocean models; i.e., at the upper boundary, the freshwater flux is specified to be constant, but the heat flux is proportional to the difference between a given constant equivalent atmospheric temperature and the top level ocean temperature. This can result in a large variability of the thermohaline circulation, as discussed by Weaver and Sarachik (1991a,b), including variability on a decadal time scale. Recently Huang and Chou (1994), and Greatbatch and Zhang (1993) have described interdecadal oscillations in models driven under constant flux boundary conditions. Greatbatch and Zhang showed the similarity between an oscillation driven by constant heat flux and the interdecadal oscillation found in the GFDL coupled model (Delworth *et al.,* 1993).

In this paper, we couple a thermodynamic sea ice model (Semtner, 1976) to the planetary geostrophic ocean circulation model of Zhang, Lin and Greatbatch (1992, hereafter referred to as ZLG). We focus on the most important thermodynamic effects associated with changes in ice cover: the insulation effect of an ice cover which affects the surface heat flux, and salinity rejection/dilution which modifies the freshwater flux seen by the ocean. In addition, we allow for changes in this freshwater flux by letting some be taken up as snow accumulation on top of the ice. The dynamic effect of the sea-ice is not considered, and is left for future work, although we recognize this may be important. For example, Hakkinen (1993) has discussed sea ice export from the Arctic as a possible source of the Great Salinity Anomaly (Dickson *et al.,* 1988). We also simplify our model by using annual mean forcing with no seasonal cycle. Seasonally varying forcing may be required for a more detailed representation of sea ice in an ocean model, but is beyond the scope of the present paper. Our aim here is to demonstrate how coupling between an ocean circulation model and a

thermodynamic ice model can lead to an interdecadal oscillation in which the thermodynamic coupling plays a crucial role.

Two studies are particularly relevant to our results; those of Welander (1977), and Yang and Neelin (1993). Welander (1977) formulated a three-box model of the air-ice-ocean system, and identified a thermal oscillation in the system which is due to a feedback between ice thickness and ocean temperature. The well-mixed ocean box is characterized by a uniform temperature with no dynamics. Yang and Neelin (1993) formulated a two-dimensional latitude/depth ice-ocean model by coupling the linearized version of Welander's (1977) ice model to the zonally averaged ocean model of Marotzke *et al.* (1988). Their results show an oscillation of period 13.5 years, due to a feedback between the thermohaline circulation and the salinity rejection/dilution associated with the freezing/melting of sea ice. Yang and Neelin restored the top level temperature below the ice to a given temperature of $-2°C$, thus limiting the thermal coupling of the ice-ocean system. In our study, we use a more complete thermodynamic sea ice model. This is fully coupled to our three-dimensional planetary geostrophic model, including a detailed representation of the thermal insulating effect of sea-ice. The results are interpreted in terms of the oscillation found by Welander.

There have been previous coupled ice-ocean modelling studies, although none of these consider the coupling of sea-ice to the large scale thermohaline circulation. For example, Hibler and Bryan (1987) coupled the dynamic-thermodynamic sea ice model of Hibler (1979, 1980) to a 14-level baroclinic Bryan-Cox ocean model (Bryan, 1969; Cox, 1984). The temperature and salinity in all model levels except the topmost were damped to climatological values with a 3-year relaxation time scale. The thermohaline circulation was constrained both by the damping term and the limited high latitude model domain. Semtner (1987) removed the damping term and modelled the Arctic Ocean and Greenland Sea with specified constant inflows. Apart from this specification, interaction with the ocean outside the model domain was excluded. More recently, Hakkinen and Mellor (1992) have described the seasonal variability of a coupled Arctic ice-ocean model. We note that Saltzman (1978) identified the sea ice-ocean temperature feedback mechanism in a simple oscillator model. This mechanism was also included in subsequent models of climatic feedback on century and longer time scales involving sea ice extent, ocean temperature and carbon dioxide concentration (Saltzman and Moritz, 1980; Saltzman *et al.*, 1981; Saltzman, 1982).

The following section describes the formulation of the ice model and the treatment of the surface heat and fresh water fluxes. Sections 3 and 4 describe respectively the results obtained under restoring and mixed surface boundary conditions. Further discussion of the results using conceptual models are presented in Section 5, and the conclusions are given in the final section.

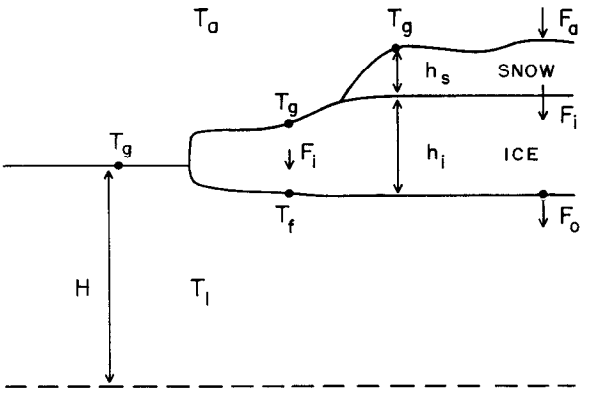

Figure 1. A schematic diagram of the coupled ocean-ice-snow system, indicating model parameters discussed in the text.

2. Formulation of the ice model and the treatment of the surface heat and freshwater fluxes

The ice model used here is basically the same as Semtner's (1976) zero-layer thermodynamic model including snow cover; this in turn is a simplification of a more complete many-layer thermodynamic ice model of Maykut and Untersteiner (1971). Further details of this type of model can be found in the original references. Here, we describe briefly the ice model, emphasizing the processes included and the parameters used. The code has been verified with a 30 m deep mixed layer ocean and seasonal forcing, by comparing the results with Semtner (1976). The ice model is coupled to the planetary geostrophic model of ZLG, by an interactive calculation of the heat and salinity fluxes at the ice-ocean interface which we now describe in detail.

The ice model has one snow layer and one ice layer, and no penetration of solar radiation is allowed in either layer. The ice and snow distribution within one grid cell has uniform depth with no leads. The sensible heat storage in ice and snow, and the latent heat in the brine pockets within the ice, are neglected; there is thus no need to calculate the temperature within ice and snow. There is no consideration of ice dynamics; the model is thermodynamic only.

The heat fluxes between the atmosphere and ice/snow, within the ice and snow, and between the ice and the ocean, are denoted by F_a, F_i and F_o respectively. A downward heat flux is positive. Figure 1 shows a sketch of the various fluxes. The rate of change with time (t) of ice (h_i) and snow (h_s) thicknesses, with density ρ_i and ρ_s respectively, is determined by the following equation.

$$-L_f \frac{\partial(\rho_i h_i + \rho_s h_s)}{\partial t} = (F_i - F_o) + I_m. \tag{1}$$

The first term on the right-hand side is the ablation or accretion at the bottom of the ice due to the difference between the heat flux F_o seen by the ocean at the ice-ocean

interface and the conductive flux within the ice or snow F_i; the latter is assumed to be constant in the vertical direction. L_f is the latent heat of fusion. The second term on the right-hand side is $I_m = F_a - F_i$, which is never negative, as it represents the melting of snow or ice at the upper surface. Snow is first melted, and any amount of heat left over is used to melt the ice underneath.

The oceanic flux F_o is given by

$$F_o = K_{iw}(T_f - T_1) \tag{2}$$

where T_1 is the top level ocean temperature, and $T_f = -1.6°C$ is the temperature at the ice-water interface and corresponds to the freezing point of sea water. The value of the transfer coefficient K_{iw} is subject to some uncertainty and various values have been used by different researchers; here, we use $K_{iw} = 180$ W m^{-2} K^{-1}. The model results are not sensitive to its precise value, as long as it is between 125 and 250 W m^{-2} K^{-1}. F_i is the conductive heat flux within the ice and is given by

$$F_i = K_c(T_g - T_f)$$

where T_g is the skin temperature at the uppermost ice or snow surface. K_c is the combined bulk conductivity of ice and snow, and depends on the ice and snow depths.

$$\frac{1}{K_c} = \frac{h_i}{k} + \frac{h_s}{k_s}$$

The value of the ice conductivity is $k = 2$ W m^{-1} K^{-1}. The snow conductivity $k_s = 0.3$ W m^{-1} K^{-1} is much smaller. We define an effective conductive depth (h) which equals a weighted average of the ice and snow depths.

$$h = h_i + \frac{k}{k_s} h_s.$$

Henceforth, we refer to h as the ice depth. The conductive flux within ice, taking into account the presence of snow, is then

$$F_i = \frac{k}{h}(T_g - T_f). \tag{3}$$

For the upper surface of either snow or ice, an instant balance between the net atmospheric flux (F_a) and the conductive flux (F_i) is first used to obtain the surface temperature of the snow or ice (T_g). If the latter is less than the freezing point ($T_g < T_f$) then $I_m = F_a - F_i = 0$ and there is no melting. However, when the surface temperature T_g obtained is higher than the freezing point ($T_g > T_f$), and with ice or snow present, the surface temperature is reset to the freezing point, and the flux imbalance due to this re-arrangement is used to melt snow. If all the snow is melted

or if there is no snow, the remaining unused flux is used to melt ice. This results in non-zero values of the melting term I_m.

We now turn to the atmospheric flux (F_a) at the upper boundary of the system. In the case of an ice- and snow-free ocean, this can be represented as the difference between an equivalent atmospheric temperature (T_a) and the sea surface temperature (T_g) (Haney, 1971); the latter is assumed to be the same as the top ocean level temperature T_1 for the open ocean. There are difficulties when a similar linear equation is used to represent heat fluxes over an ice covered ocean. The range of the surface temperature (T_g) over ice can be much larger than that over ocean, thus the linear approximation for the long wave radiation is not as accurate. The change in parameters such as the albedo is discontinuous between ice-covered and ice-free states. We thus introduce an "albedo" temperature of ice or snow (T_i, T_s), but still use the linear approximation, in order to lower the equivalent atmospheric temperature from its value if ice or snow were not present. The equivalent atmosphere temperature T_a is thus defined as

$$T_a = T_a^* + T_i + T_s$$

where T_a^* is the equivalent atmospheric temperature in the absence of ice or snow. It should be less variable than T_a since the change due to ice and snow cover is already accounted for by the term $T_i + T_s$. We thus specify T_a^* as being independent of time for our annual mean forcing. The atmospheric flux F_a is then

$$F_a = D(T_a - T_g). \tag{4}$$

This linear parameterization, without the T_i and T_s terms, has been used by Roed (1984) to study the lateral ice growth at marginal ice zones, and by Welander (1977) in his idealized, theoretical model. In Eq. (4), D is the feedback coefficient which determines the time scale of the relaxation of the surface temperature (T_g). The parameters T_i and T_s take on non-zero values only when the ice and snow depth exceeds a given minimum value: $T_i = -4°C$ and $T_s = -2°C$ for ice and snow depths exceeding 10 cm and 8 cm respectively. In open ocean regions, (4) is applied with $T_g = T_1$, the top level ocean temperature.

We now specialize to the case with no melting at the air-ice/snow interface, $I_m = 0$. This is almost always the case in our simulations due to the use of a constant annual mean T_a^*; as can be verified from our results. When $I_m = 0$, the thermodynamic ice model used here is identical to that of Welander (1977). Using Eq. (3)–(4) with $I_m = 0$ (i.e. $F_a = F_i$), the two unknowns T_g and F_i can be obtained as follows.

$$T_g = T_f + \frac{hD/k}{1 + (hD/k)}(T_a - T_f) \tag{5}$$

$$F_i = \frac{D}{1 + (hD/k)}(T_a - T_f). \tag{6}$$

The case of vanishing ice depth ($h = 0$) is not a singular point in the above equations; thus the use of a minimum ice depth is not necessary.

Note that the inverse depth $D/k = (4\text{ cm})^{-1}$, for the parameter values $D = 50$ W °C^{-1} m^{-2} and $k = 2$ W °C^{-1} m^{-1}. For relatively large ice depths ($hD/k \gg 1$), the surface temperature T_g is close to, and thus sensitive to the atmospheric forcing temperature T_a. The flux F_i is however not sensitive, as it is almost zero. Physically, this describes the insulating effect due to thick ice. For small ice depths ($hD/k \ll 1$), the value of T_a is important in determining the magnitude of the heat flux F_i, but has little effect on T_g, as the latter is close to the freezing point (T_f). In terms of the surface temperature and the heat flux, the reference ice depth of 4 cm thus separates the ice-covered and ice-free regimes. Since the insulation effect only applies to the ice covered region, including leads would weaken the insulation effect and thus increase the reference ice thickness.

The rate of change of the heat flux (F_i) with ice depth (h) is given by

$$\frac{\partial F_i}{\partial h} = \frac{-D/k}{1 + (hD/k)} F_i. \tag{7}$$

Figure 2 shows the conductive flux F_i as a function of ice equivalent depth h, with the flux at $h = 0$ specified to be -100 W m^{-2}. The rate of change of the flux with h is also shown. The flux change is sensitive to h when the latter is small, and this sensitivity is reduced when h is large, as the flux itself becomes small then.

Having discussed the handling of the surface heat flux boundary condition, we now turn to the treatment of the freshwater flux. The model is first spun-up using restoring boundary conditions on both temperature and salinity. The heat flux seen by the ocean is calculated using the procedure described above; that is with the restoring condition being applied to the temperature, T_g, at the surface of the ice/ocean system (see Fig. 1). A restoring boundary condition is also applied to the salinity in the top level of the ocean model (i.e. beneath the ice). On switching to mixed boundary conditions (that is restoring on temperature and flux on salinity) we use the freshwater flux diagnosed from this spin-up. At the high latitudes affected by ice, this provides a source of fresh water for the ocean (i.e. a net excess of precipitation and run-off over evaporation). As in other studies (e.g. Yang and Neelin, 1993; Hakkinen and Mellor, 1992), we allow this freshwater to drain through the ice into the ocean, where it is then modified by the salinity rejection/dilution due to ice formation/melting. This is done by assuming the salinity of ice is 30% the salinity of sea water. In addition, some freshwater is taken up by snow accumulation, as described in the next paragraph. (In the restoring spin-up, snow is allowed to accumulate to the maximum allowed depth; in the final steady state, there is no further snow accumulation and hence snow accumulation has no effect on the diagnosed freshwater flux.) We therefore assume that river run-off and the net precipiation minus evaporation seen by the ocean is not affected by the presence of

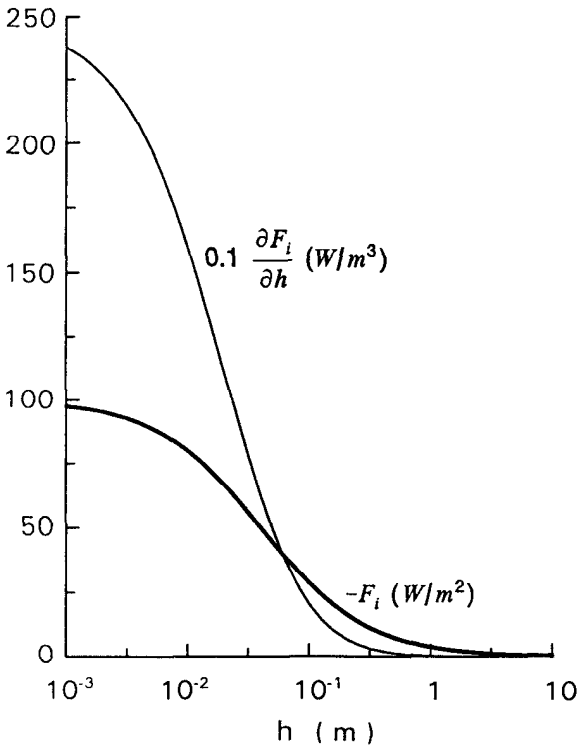

Figure 2. The conductive flux F_i (heavy line) as a function of effective conductive depth h, with the flux at $h = 0$ specified to be -100 W m^{-2}. Its rate of change with h is shown by the thin line.

ice, except in so far as some is taken up by snow accumulation. In support of this approach, it should be noted that river run-off is not necessarily limited by the presence of ice (the importance of river run-off for determining the low salinity water associated with increased ice extent has been noted by Mysak *et al.*, 1990). Also, whereas an ice cover can protect the ocean from surface precipitation, it can also limit loss of fresh water due to evaporation. Nevertheless, it is not clear how best to treat the freshwater flux and it seems sensible, at this time, to take the simple approach adopted here, and hope that ways to improve it can be found in the future.

A fixed snow fall of 5 cm per month is prescribed when the ice thickness reaches a minimum of 0.1 m and when the surface temperature is below freezing, up to a maximum limit of 0.15 m. When the model is run under mixed boundary conditions, this snow fall is removed from the freshwater flux seen by the ocean. A limit for the snow depth is necessary since the surface forcing is held constant; thus the diurnal and seasonal cycles and synoptic variability, which ordinarily would play a role in limiting the snow depth, are ignored. Snow-ice conversion processes such as melting and refreezing, are also neglected. If no maximum snow limit were imposed, the

Table 1. Depths at the bottom of each model level.

Level number	Depth
1	46 m
2	104
3	177
4	269
5	385
6	531
7	715
8	947
9	1239
10	1607
11	2070
12	2654
13	3327
14	4000

snow depth would keep increasing. As the insulating effect of snow is several times larger than that of ice for the same depth, the large snow depth would eventually reduce the atmospheric heat flux to much smaller than the oceanic flux, and the latter would melt all the ice. In this case, all the snow would fall into the ocean, and this unrealistic cycle would start again by ice formation and snow accumulation.

3. Spin-up under restoring surface boundary conditions

The experimental conditions and model parameters are the same as those in Zhang, Greatbatch and Lin (1993, hereafter ZGL), except that the equivalent atmospheric temperature, T_a^*, used for the restoring boundary condition on temperature is lowered to allow for ice formation. The flat bottomed model domain has an extent of 60 degrees latitude and longitude, from 5 to 65 N. There are 14 levels in the vertical with 7 of them lying above a depth of 700 m, and the depth of the top level is 46 m. The depths of the bottom of each level are given by Table 1. The simplified equation of state is given by:

$$\rho(T, S) = 3.0 + 0.77S - 0.072T(1 + 0.072T). \tag{8}$$

Here, T is temperature in °C, S is salinity in ‰, and ρ is density in units of kg m^{-3} and reduced by 1000. The coefficients in Eq. (8) are similar to those of Bryan and Cox (1972); compressibility effects are ignored.

The equivalent atmospheric temperature distribution (T_a^*) which is used to force the coupled ice-ocean model is shown in Figure 3. It is identical to that used in ZGL, except we include an additional term which vanishes at the southern boundary of 5 N and which linearly decreases to −5°C at the northern boundary of 65 N. This is a more realistic profile than that used by ZGL, as we no longer need to avoid

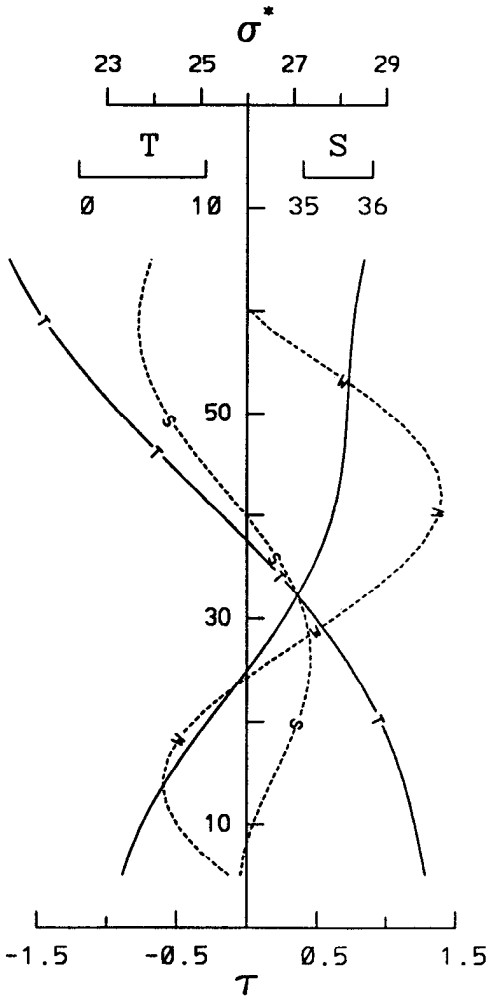

Figure 3. The latitudinal (φ; °N) distributions of the equivalent atmospheric temperature (curve T; °C), salinity (curve S; ‰) and density (unlabelled curve; σ-unit). The latter is calculated using the equation of the state, Eq. (8). Curve W is the surface wind stress (τ, dynes cm^{-2}).

sub-freezing temperatures with the inclusion of an ice model. The high latitudes are now sufficiently cold that ice formation is possible in the control equilibrium state. The latter is obtained by spinning up the model for several thousand years to a quasi-steady state, using restoring conditions on both temperature and salinity, as described in detail in the previous section. The salinity profile used for the restoring spin-up is shown in Figure 3. The relaxation time for the surface forcing is 30 days, the same as in ZGL. The other model parameters are listed in Table 2.

Table 2. Model parameters.

ρ_i	ice density	910 kg m^{-3}
ρ_w	water density	1025 kg m^{-3}
L_f	latent heat of fusion	3.34×10^5 J kg^{-1}
k	ice conductivity	2 W m^{-1} K^{-1}
k_s	snow conductivity	0.3 W m^{-1} K^{-1}
C_p	specific heat of water	4180 J kg^{-1} K^{-1}
α	thermal expansion coefficient	-0.072 kg m^{-3} K^1
β	salinity expansion coefficient	0.77 kg m^{-3} $‰^{-1}$
K_{iw}	transfer coefficient at ice-water interface	180 W m^{-2} K^{-1}
T_f	freezing temperature of sea water	-1.6°C
T_i	'albedo' temperature of ice	0 or -4°C
T_s	'albedo' temperature of snow	0 or -2°C
D	relaxation coefficient for atmospheric heat flux, for top model level of depth 46 m	30 days
H	top model level depth	46 m
$\mathscr{H}$	total depth of ocean	4000 m
Θ	average depth of ice	1 m
A_H	horizontal diffusivity	2000 m^2 s^{-1}
A_v	vertical diffusivity	0.63×10^{-4} m^2 s^{-1}

The nine panels of Figure 4 describe the circulation of this equilibrium state. Note that each tick mark in the vertical represents the center of the level, and the depth of the bottom of each level is given in Table 1. This distortion of the vertical coordinate enables an expanded and clearer view of the upper ocean. The upper block shows the latitude/depth plots of the zonally averaged density, temperature, salinity and meridional overturning streamfunction; the lower block shows the longitude/latitude plots of the temperature at the surface of the ice ocean system, the top level salinity, ice depth, depth of convective overturning (number of adjacent levels which undergo convection), and the surface heat flux (diagnosed and averaged over the final 3 months of model integration). The corresponding surface salt flux is shown in Figure 5.

4. Results obtained with mixed surface boundary conditions

ZGL spun up an ocean-only model, very similar to the one in this paper, using restoring temperature and salinity surface boundary conditions. A switch was then made to mixed conditions, i.e., restoring on temperature and flux on salinity, and the polar halocline catastrophe ensued, as described by Bryan (1986a). The high latitude convection was almost eliminated due to the amplification of an initially imposed small fresh water perturbation, which leads to a fresh water cap and the resulting shutdown of the thermohaline circulation. ZGL showed that the accompanying reduction in surface heat flux is crucial to the occurrence of the catastrophe. As we saw earlier, the insulating effect of ice also significantly reduces the air-sea heat flux.

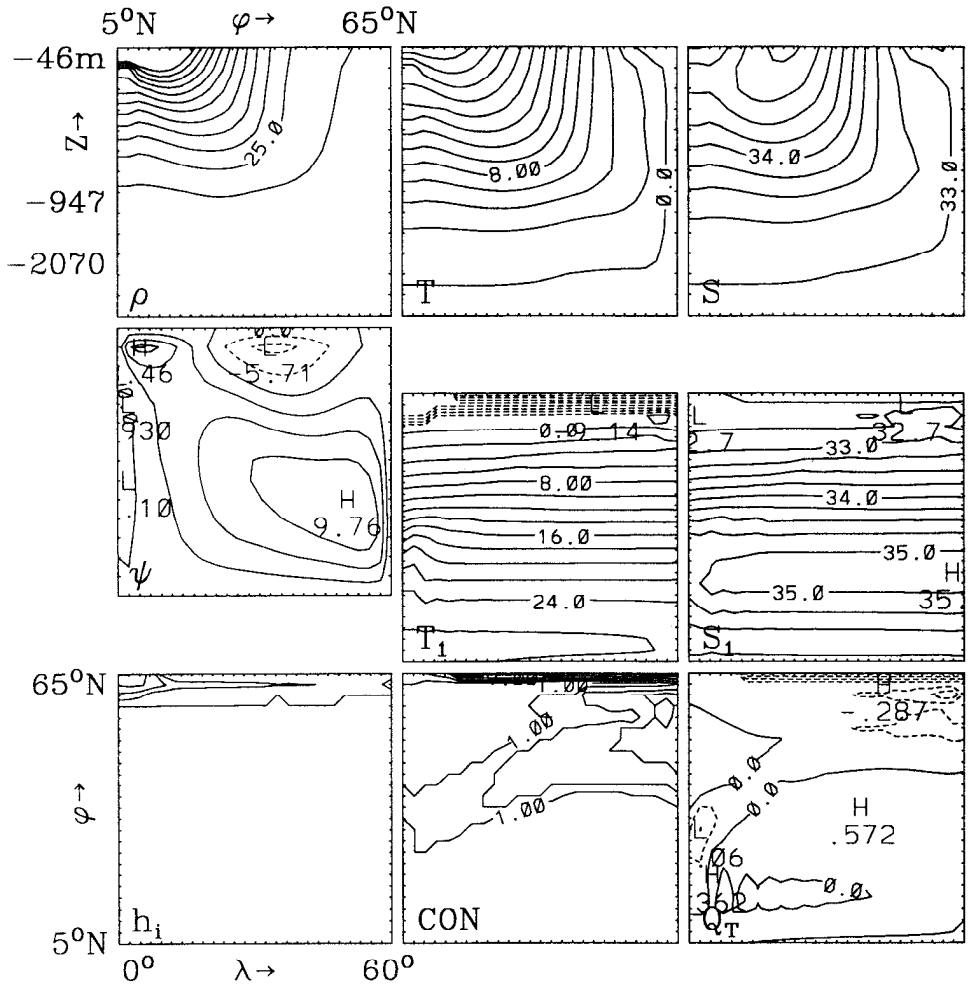

Figure 4. Steady state obtained with restoring conditions on both surface temperature and salinity. The upper block consists of latitude (φ)/depth (z) plots: the zonally averaged density (ρ; the contour interval is 0.25 σ-unit), temperature (T; 2°C), salinity (S; 0.25‰) and meridional overturning stream function (ψ; 2.5 Sv). The lower block consists of longitude (λ)/latitude (φ) plots: the temperature (T_1; 2°C) at the surface of the ice ocean system, salinity (S_1; 0.25‰), ice depth (h_i; 0.5 m, with the southernmost contour being 0 m), depth of convective overturning (CON; number of adjacent levels which undergo convection, every 2 levels contoured), and surface heat flux (Q_T; 0.5°C month^{-1} for the top model level of 46 m depth). This state serves as the initial condition for subsequent numerical experiments.

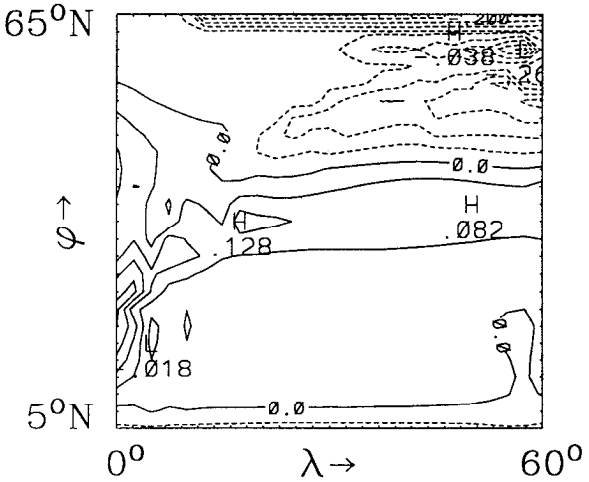

Figure 5. The surface salt flux (Q_s; 0.05‰ month^{-1} for the top model level of 46 m depth) diagnosed from the steady state of Figure 4. This flux is used to provide the surface boundary condition for salinity under mixed boundary condition.

We thus repeat ZGL's experiment by changing from restoring to mixed conditions, but starting from the steady state obtained with the ice-ocean model shown in Figure 4.

Instead of the complete collapse of the thermohaline circulation found by ZGL, an oscillation with a period of about 17 years is found. Figure 6 shows a time series of the fractional ice coverage and the basin mean temperature. Three such cycles are shown in more detail in the inset. After an initial adjustment upon the switch of the surface boundary conditions, the model simulates a stable sequence of these oscillations. In Figure 7, we show various oceanic parameters at different times during the oscillation, starting from a reference time of $t = 0$, which is 507.5 years after the switch to mixed boundary conditions, and then at times $t = 2.5$, 7.5 and 12.5 years. The sequence starts with the ice cover at its largest extent with a maximum depth of 2.6 m and sub-freezing surface temperatures, T_1, over the entire northern basin (Fig. 7a). The thermal insulation of the ice cover means that the surface heat loss and convective activity are at a minimum, as evidenced by the northward, subsurface bulging of the outcropping isotherms. The thermohaline circulation is at its peak intensity of over 14 Sv at this time, with the downwelling concentrated in a narrow band along the northern wall (Fig. 7a), despite the fact that convective activity is at a minimum.

Since the ice cover is a maximum, the thermal insulation effect allows the ocean to warm up as a result of the largely unchanged air-sea heat flux at lower latitudes (note the phase difference between the ice extent and the basin mean temperature in

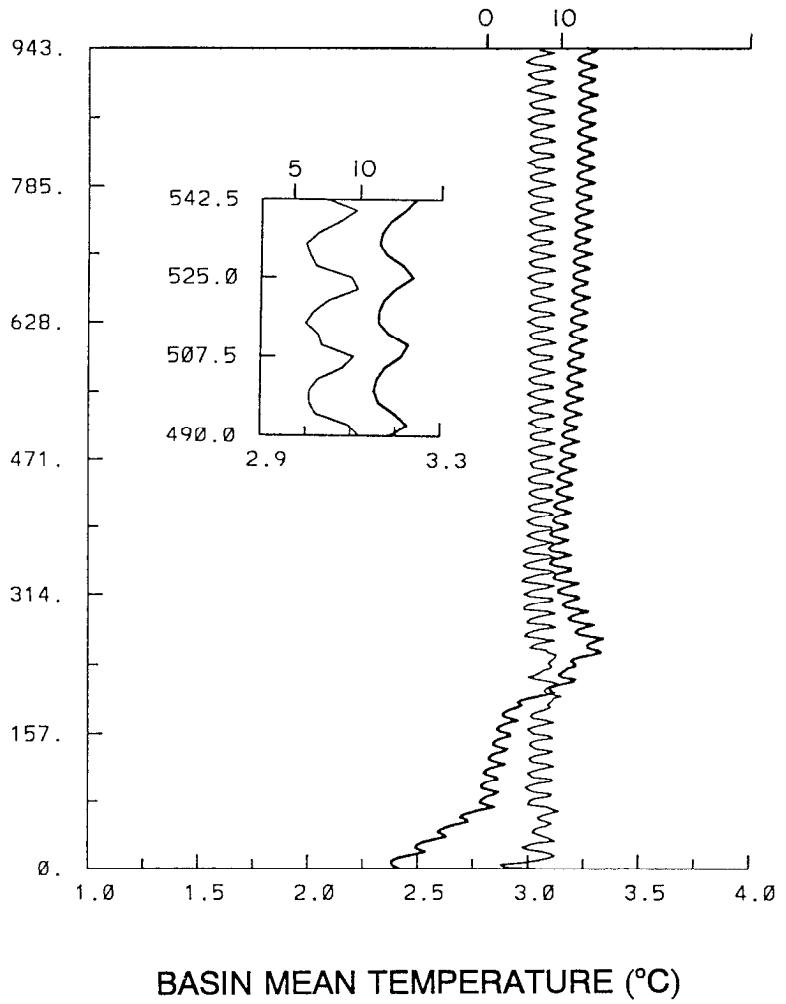

Figure 6. Time series of the basin averaged ocean temperature (°C, heavy line) and the fractional ice coverage (light line). The inset shows three cycles in more detail.

Figure 6, with the ice extent leading). Since the thermohaline circulation is at its peak strength when the ice cover is a maximum, this heat is carried northward under the ice. The water column is then destabilized, leading to an onset of deep convection and a melting of the ice, resulting in a negative feedback mechanism. This results in

an overall reduction of ice thickness and ice extent in the northeastern part of the basin at $t = 2.5$ years (Fig. 7b), with much enhanced heat loss to the atmosphere. The enhanced deep convection can also be seen at the same location. Evidence of this convection is the upward doming of the isopycnals (e.g., $\sigma = 25.0$) that can be seen in the zonally-averaged density, and the homogenized temperature of the water column at the same latitude. In the meantime, the thermohaline overturning is beginning to weaken.

The reduction of ice thickness and ice extent continues to time $t = 7.5$ years (Fig. 7c). The ice thickness and extent, as well as the thermohaline circulation is about to reach its minimum and the region of heat loss is approaching its largest extent. The high latitude heat loss then leads to ice growth, a reduction in deep convection and a gradual enhancement of the thermohaline circulation. This can be seen at $t = 12.5$ years (Fig. 7d); the ice cover is also extending eastwards. Once the ice extent has reached its maximum, the cycle repeats itself. It is an interesting feature of the oscillation that the maximum in the thermohaline circulation occurs when the deep convection is at a minimum, and vica versa. This shows that the thermohaline overturning does not respond instantly to changes in deep convection (a topic of current research). What is important here is to note that the thermohaline circulation plays an important role in transporting heat under the ice and is a necessary feature of the oscillation.

We now examine the effect of the presence of an ice cover in more detail. Four factors need to be considered: the change in the equivalent atmospheric temperature T_a due to the albedo parameters T_i and T_s; the thermal insulation effect of an ice cover; the salinity rejection/dilution accompanying ice formation/melting; and snow accumulation. The former two relate to the air-sea heat flux, while the latter two change the salinity of surface water (snow accumulation affects salinity since it takes up some of the freshwater flux; it also increases the insulating effect of the ice-snow layer). Through their effect on density, they all affect the buoyancy flux from the deep ocean, which is dominated by convection.

With an ice cover, the change in the equivalent atmospheric temperature is important in determining the surface temperature T_g, but it is not crucial for the ocean circulation, because the heat flux is small (Eq. 6) when the ice and snow depths are sufficient for the albedo parameters to take effect. Indeed, keeping the equivalent atmospheric temperature constant (by putting $T_i = T_s = 0$) does not significantly change our results. The important factor is the change in the heat flux that occurs in response to changes in ice extent because of the insulation effect of the ice.

For annual mean surface forcing, we shall argue in the next section that salinity rejection/dilution is of secondary importance. We have verified this by removing this effect from our model and then repeating the experiment. The result is an oscillation that differs little from what we have described. The reason is the dominating influence of changes in convective fluxes, associated with deep convection, for

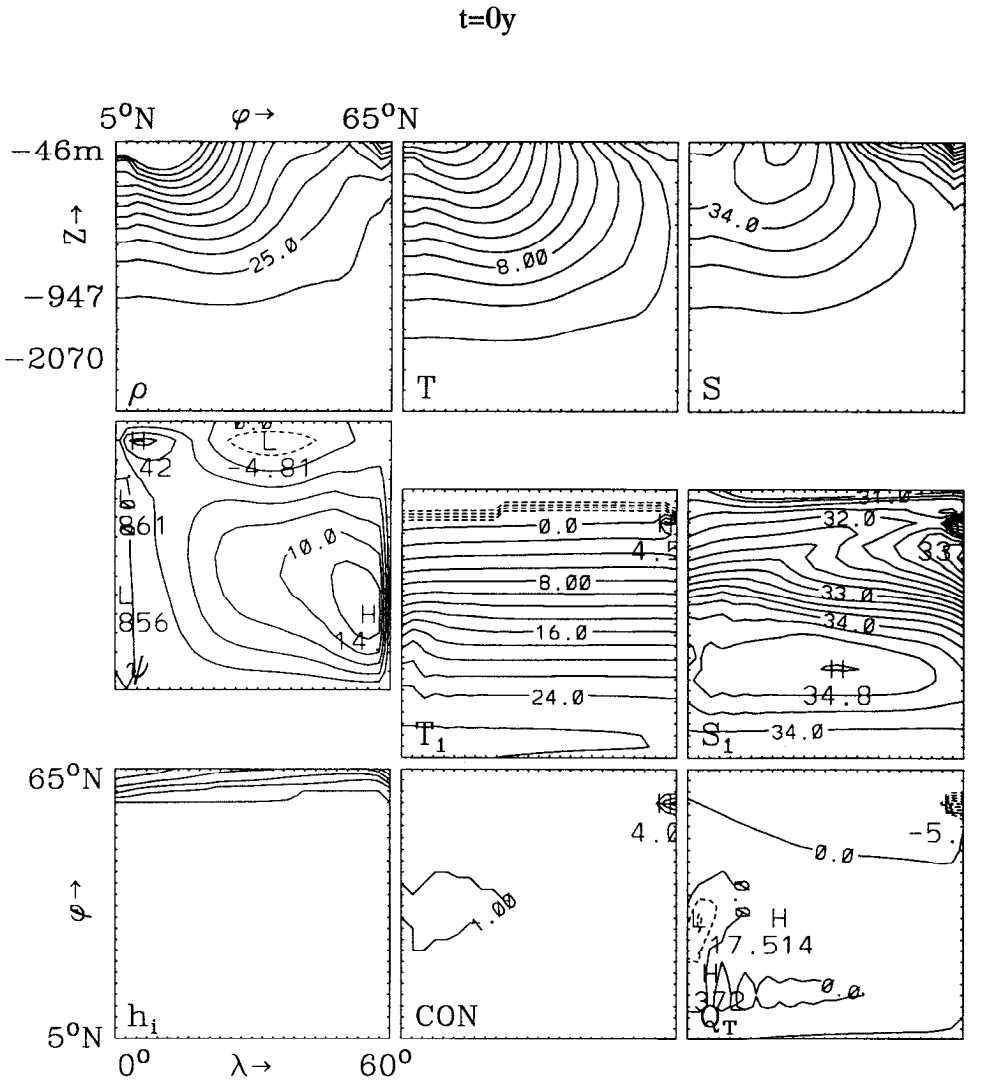

Figure 7. Model variables, illustrating the oscillation obtained under mixed boundary conditions, at times t = (a) 0 y, (b) 2.5 y, (c) 7.5 y and (d) 12.5 y. The display format is the same as in Figure 4. Time $t = 0$ is the time of maximum ice extent. The oscillation period is 17 years.

determining the surface salinity beneath the ice. During ice formation, especially when the ice cover is advancing, the cooling flux to the atmosphere is reduced (Eq. 6). This in turn means that the convective and diffusive heat flux from the deep ocean must be reduced even more, since otherwise, there would be no heat flux divergence at the base of the ice (the $F_i - F_o$ term in Eq. 1) and no ice growth, contradicting our assumption that ice growth is indeed ocurring. This means that the density of the

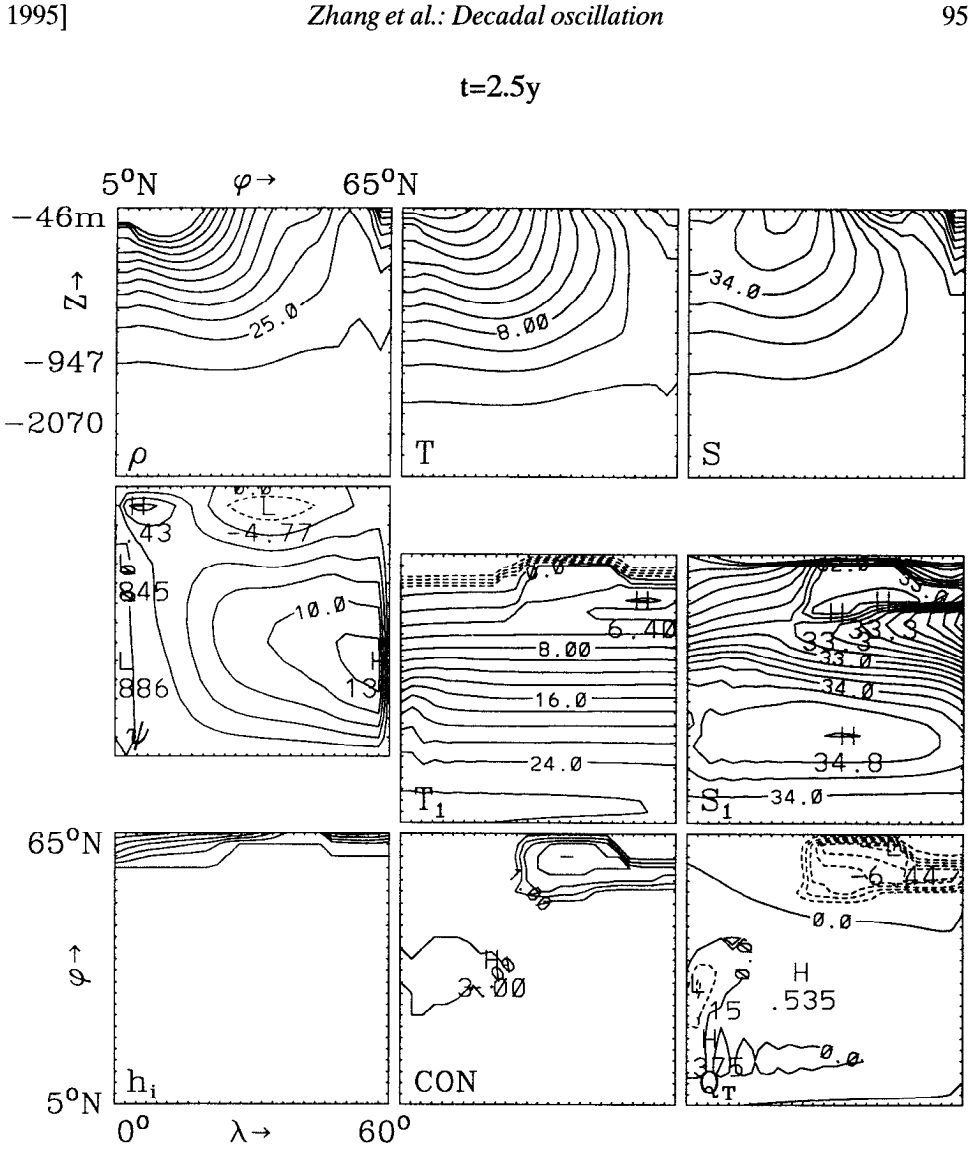

Figure 7. (Continued)

surface level waters below the ice must be less than before, and so cannot be dominated by salinity rejection. A consequence is that regions of increased ice extent in our model are also associated with reduced surface salinity (this can be seen in Fig. 7).

Manak and Mysak (1989) found from a sea ice data analysis that there was a large decrease in the salinity of the Labrador Sea for those years when the ice extent was 30% greater than average. In addition, Marsden *et al.* (1991) found a significant negative correlation between the ice anomaly and near surface salinity using data

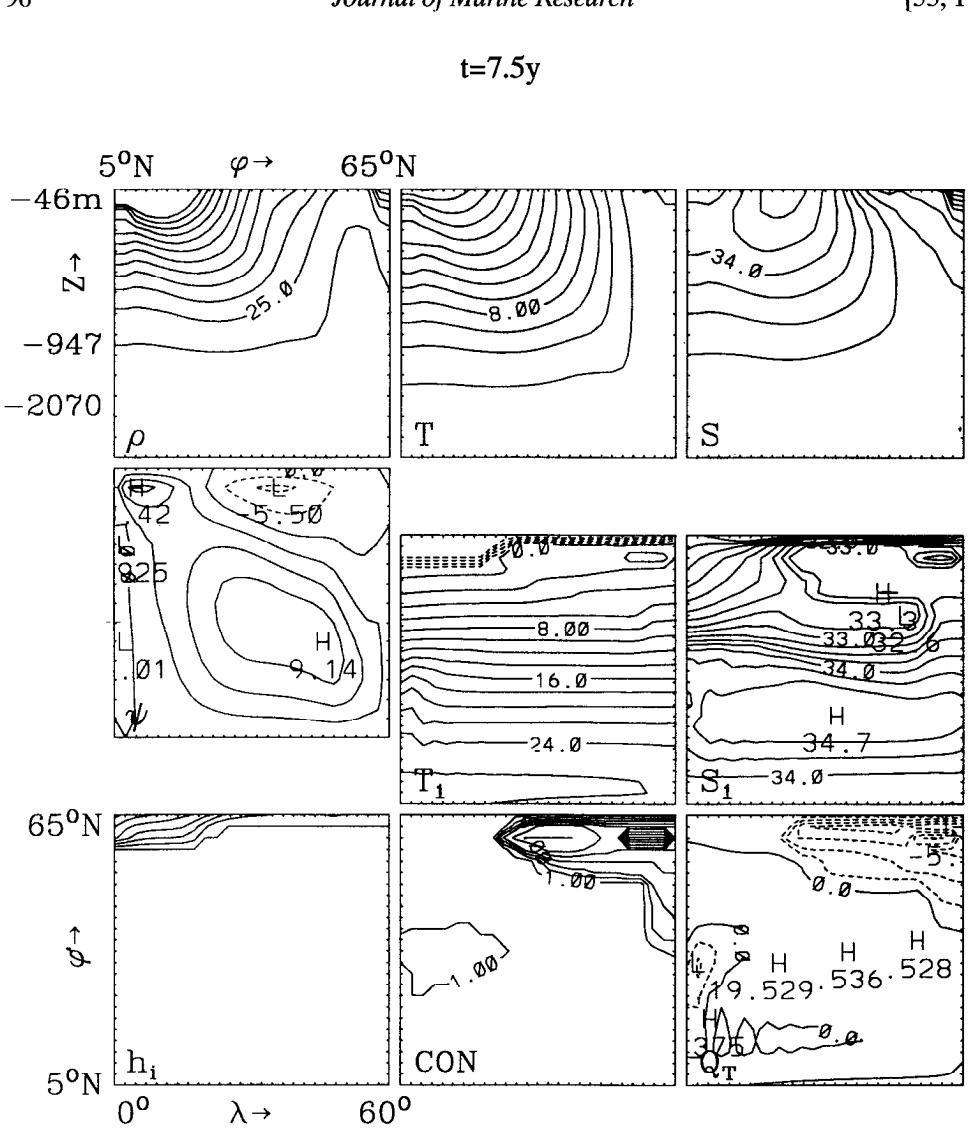

Figure 7. (Continued)

from the high latitude North Atlantic Ocean. This is consistent with our finding that salinity rejection is not of primary importance. It also indicates that a source of fresh water is needed that allows the salinity to reduce as the ice extent grows. This provides some justification for the simple treatment we have used to apply the freshwater flux boundary condition (see the discussion in Section 2), since at high latitudes, our diagnosed flux (shown in Fig. 5) provides a source of fresh water to the ocean. A large part of this flux should probably be interpreted as river run-off. This is

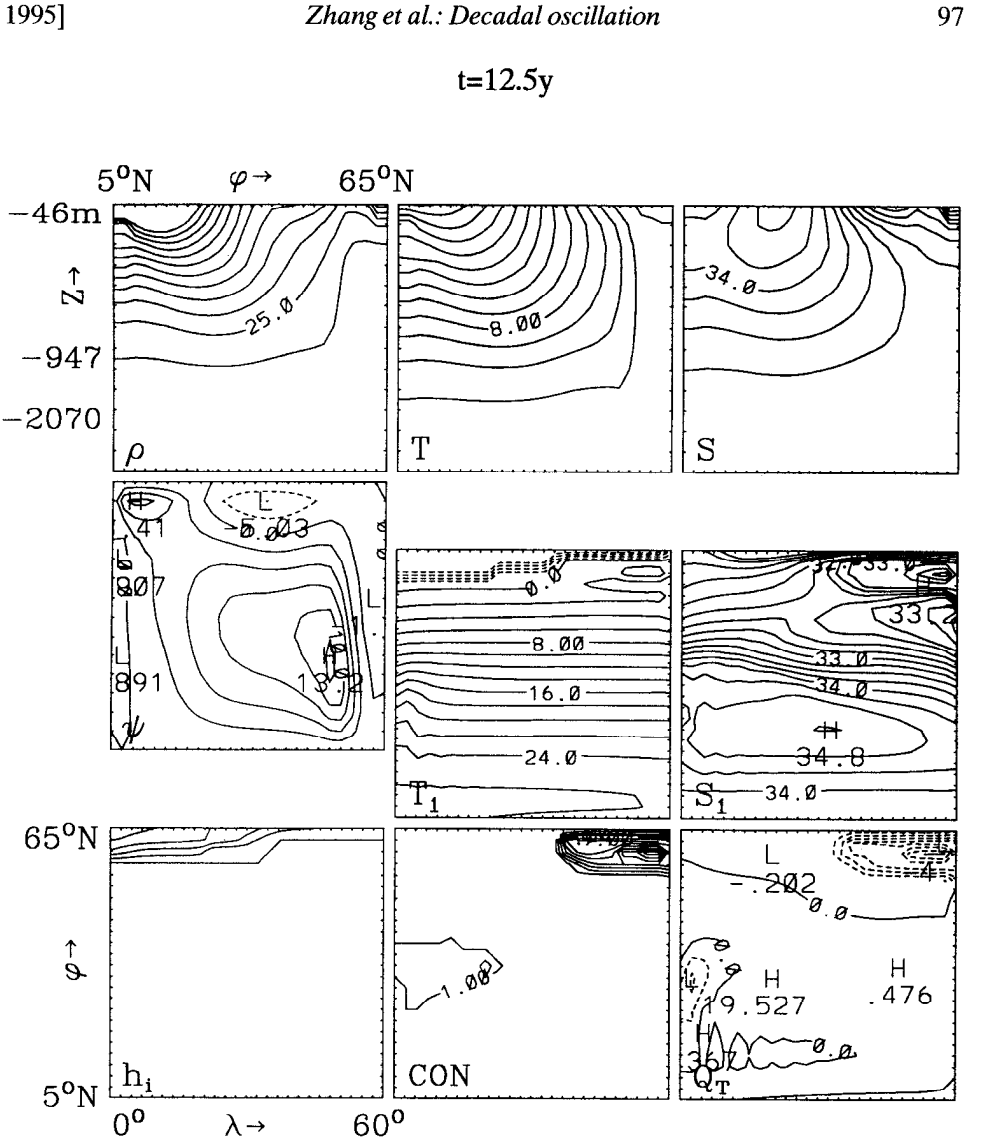

Figure 7. (Continued)

consistent with the importance attached to river run-off in the analysis of Mysak *et al.* (1990), except that in their case it is the anomalies of run-off that are important.

Another question concerns the sensitivity of the oscillation period to the model parameters. Changing the restoring time for the top level temperature from 30 to 50 days, through the parameter D in Eq. (4), increases the period of the oscillation from 17 to nearly 30 years. In Section 5, we show that this is because increasing the restoring time scale decreases the change in surface heat flux that occurs during the

ice advance and retreat (the surface heat flux in the control equilibrium state is also weaker in this case).

5. Further discussion of the results

In this section, we present conceptual models to interpret the model results. The thermodynamic effect responsible for the oscillation can be captured by a simple anomaly model involving the two diagnostic quantities of anomalous fractional ice coverage (C), and anomalous basin averaged ocean temperature, denoted as simply T here. Averaging the governing temperature equation given in ZLG, we see that the only mechanism to change the basin averaged temperature is through an anomalous horizontally averaged air-to-sea surface heat flux. This is because the side and bottom boundaries of the basin are insulating, and advection, diffusion and convection only redistribute heat. To represent the thermal insulating effect of an ice cover in our conceptual model, we assume the difference in surface heat flux between an ice-covered and ice-free ocean (ΔF) together with the anomaly ice cover (C), determine the change in the basin averaged temperature: increasing ice cover would lead to a larger net air-to-sea flux. This is consistent with the fact that ice forms only in regions of the ocean where there is a net heat loss to the atmosphere.

$$\rho_w C_p \mathscr{H} \frac{\partial T}{\partial t} = \Delta F C. \tag{9}$$

Here, $\mathscr{H} = 4000$ m is the total depth of the ocean. To close the model, we note that an anomalously cold ocean would lead to an anomalously large ice cover, thus

$$\rho_i \Theta L_f \frac{\partial C}{\partial t} = -K'_{iw} T. \tag{10}$$

This is basically Eq. (1) with a fixed ice depth, in anomaly form. Here, Θ is a mean ice depth and K'_{iw} is an effective transfer coefficient between ice and water, which should be much less than the value of $K_{iw} = 180$ W °C^{-1} m^{-2} used in Section 3, since the temperature here is the basin averaged value, and not the top level temperature immediately below the ice. Combining Eq. (9) and (10), we obtain

$$\frac{\partial^2 C}{\partial t^2} = -\omega^2 C, \qquad \omega_2 = -\frac{K'_{iw} \Delta F}{\rho_i \Theta L_f \rho_w C_p \mathscr{H}}.$$

We see that sinusoidal solutions for the ice coverage and basin average temperature would result, with a phase difference of 90° between them. Analysis of the time series of Figure 6 shows that the ice cover leads the temperature by about 45° in our planetary geostrophic model; the discrepancy from the value of our conceptual thermodynamic model is probably due to dynamical effects, such as the transport of

heat by the thermohaline circulation under the ice, something we have seen to be important.

To calculate the period of oscillation, we take as parameter values, $\Theta = 1$ m and $\Delta F = 50$ W m^{-2}, with the value of K'_{iw} (W °C^{-1} m^{-2}) to be determined later. A list of the values of the constants used is given in Table 2. The period of the oscillation is then

$$\frac{2\pi}{\omega} = \frac{64}{\sqrt{K'_{iw}}} \text{ (years)}.$$

If we scale down the effective transfer coefficient (K'_{iw}) by one order from the standard value of $K_{iw} = 180$ W °C^{-1} m^{-2}, corresponding to a reduced efficiency of heat transfer, we obtain a period of 15 y. Due to the square root dependence of the coefficient, the exact period will still be decadal over a wide range of the values of the coefficient. The period as simulated by our planetary geostrophic model is sensitive to the value of the parameter D associated with the time scale of the surface thermal forcing, since the magnitude of the ΔF increases with D. Changing the time scale from 30 to 50 days results in a change of the simulated period from 17 to nearly 30 y. The phase difference remains at about 45°.

Welander (1977) showed that a self-sustained oscillation can be obtained with a 1-dimensional vertical ice-ocean model with no salinity effects. The phase difference between the temperature and ice depth variation in his model as estimated from his Figure 4 is about 60°, close to our simulated value of 45°. This mechanism of a self-sustained oscillation is quite different from that proposed by Yang and Neelin (1993); the latter involves a positive feedback between the thermohaline circulation and the formation of ice, which is associated with salinity rejection. In our simulations, brine rejection during ice formation can be suppressed with little change to the model results, as we have already noted. This shows that the main mechanism at work in our case is the thermal insulating effect of the ice cover.

To further assess the relative importance of salinity rejection during ice formation and the insulating effect of an ice cover on the density, we use another conceptual anomaly model. The basic assumptions are as follows.

(a) The system in consideration consists of the ice layer of thickness h, and the high latitude top level of the model ocean of thickness H.

(b) The heat and salt balance is determined by the surface forcing fluxes at the top of the system, and the convective fluxes of heat (C_T) and salt (C_s) at the bottom, plus the change due to the latent heat of fusion and salinity rejection as a result of the anomalous ice thickness δh.

(c) The sensible heat storage of the top ocean model level is neglected as its temperature is always close to the freezing point; the sensible heat storage of the ice layer is also neglected as the ice depth is small compared to that of the top model level.

(d) The fractional reduction of the convective fluxes of heat and salt at the bottom of the model level is identical, since both are determined by the intensity of the convective overturning.

As a result of assumptions (a)–(c), we may express the heat and salinity balance before a change in ice cover as

$$F_i(h) + C_T = 0, \qquad SSF + C_S = 0$$

Here, $F_i(h)$ is the conductive heat flux as expressed by Eq. (6), while SSF, shown in Figure 5, is the imposed part of the surface salinity flux, and is held constant under mixed boundary conditions. The sign convention for the fluxes is that positive changes make the system warmer and saltier. The units of C_T and C_S are W m^{-2} and m s^{-1} respectively; the latter is expressed as the rate of change of equivalent fresh water depth. From assumption (c), the density change in the top level of the ocean is due to salinity change only; we thus discuss only the salinity budget in what follows.

When an anomalous ice thickness δh develops, there are corresponding anomalies in the convective heat (δC_T) and salt (δC_S) fluxes. The salinity perturbation δS is due to brine rejection on the formation of the anomalous ice thickness, and the change in the convective salt flux. The contribution to the salinity perturbation due to brine rejection (δS_1) is

$$\delta S_1 = 0.7\delta h \frac{\rho_i}{\rho_w} \frac{S_0}{H}. \tag{11}$$

Here, $S_0 = 32‰$ is the mean salinity of the top model level, and the factor 0.7 accounts for the fact that about 70% of the salt content is rejected on ice formation. The other contribution (δS_2) is due to the change in the convective salt flux.

$$\delta S_2 = \delta C_S \delta t \frac{S_0}{\mathrm{H}} = \frac{C_S}{C_T} \delta C_T \delta t \frac{S_0}{H}. \tag{12}$$

Here, δt is the duration of the anomalous convective flux. The second equality follows from assumption (d) that the fractional changes in the convective heat and salt fluxes are identical.

From assumption (b), the heat budget on ice formation is expressed as

$$\delta C_T = -\frac{\rho_i L_f \delta h}{\delta t} - \frac{\partial F_i}{\partial h} \delta h. \tag{13}$$

The rate of change of heat flux with ice depth ($\partial F_i/\partial h$) can be obtained from Eq. (7) and is positive (Fig. 2). Eq. (13) says that the release of latent heat of fusion and the reduction of heat loss to the atmosphere by the increase in ice thickness must be balanced by a reduction of the convective heat flux, in order to keep the water temperature around the freezing point.

We now need to estimate the ratio (R) of the relative contributions to the density flux from the convective salt and heat fluxes. Using the equation of state,

$$R = \frac{\beta \delta S/\delta t}{\alpha \delta T/\delta t} = \frac{\beta C_p \rho_w S_0}{\alpha} \frac{C_S}{C_T} \tag{14}$$

where α and β are the expansion coefficients for heat and salt. We now express C_S/C_T in terms of R using (14) and substitute in (12). We also substitute for δC_T from (13) in (12). The resulting expression for δS_2 gives the salinity perturbation due to changes in the convective fluxes; combining with that due to brine rejection from (11), we obtain the total salinity anomaly (δS).

$$\delta S = \delta S_1 + \delta S_2 = \frac{\delta h}{H}\left[0.7\frac{\rho_i}{\rho_w} S_0 + \frac{\alpha}{\beta C_p \rho_w} R\left(-\rho_i L_f - \frac{\partial F_i}{\partial h}\delta t\right)\right] \tag{15}$$

To understand (15) we first note that $0 < R < 1$. This ensures that the convective buoyancy flux into the surface level of the model is dominated by the heat flux, as is necessary in order to maintain convective overturning. Since $\partial F_i/\partial h > 0$ (Fig. 2), the second and third terms on the right-hand side of Eq. (15) are now seen to be both negative, and to oppose the first term which is due to salinity rejection. Numerical estimates of the three terms show that the magnitude of the first term on the right-hand side, due to salinity rejection, is more than twice as large as the second term. However, it can be cancelled by the sum of the second and third terms, which are due to anomalies in the convective fluxes, over a time scale of $\delta t \approx 10$ d, which corresponds to only several model time steps. This confirms our model result that on the decadal time scale of our oscillation (which is much greater than 10 days), salinity rejection is of secondary importance, compared to the thermal insulation of the ice cover.

It is important to note from Eq. 15 that the density change due to an increased ice amount depends on the rate of change of the ice conductive flux ($\partial F_i/\partial h$). Thus if a constant flux boundary condition is used for temperature, F_i is constant and the third term on the right-hand side of Eq. (15) would be zero. In this case, salinity rejection would determine the sign of the density change, and would be a stabilizing factor for the thermohaline circulation and ice amount through the feedback with convective overturning. We have verified this using our model with constant flux conditions on both temperature and salinity (results not shown). However, the use of the flux condition on both temperature and salinity is not realistic, as this does not allow for any changes in the flux due to the insulating effect of the ice. Another situation in which salinity rejection dominates is when the atmospheric temperature T_a is not constant, such as would happen if we included a seasonal cycle. In this case, the extra negative heat flux required to form anomalous ice in the fall and winter comes from the upper surface due to the much colder air temperature. The convective heat flux at the bottom of the system is then not constrained to decrease when ice is forming.

As the changes in the convective salt and heat fluxes are proportional, this means that the salinity flux at the bottom of the surface level is also not forced to change. In this case, salinity rejection would dominate and make the water denser. If there is only annual, but not interannual variation, in T_a, the feedback between ice amount and ocean temperature discussed in this study would still be important for the dynamics of anomalies which are over and above the regular seasonal cycle. This is consistent with the observational studies of Manak and Mysak (1989), Marsden *et al.* (1991), as discussed earlier.

6. Conclusions

We have coupled the Semtner (1976) zero-layer thermodynamic sea ice model to our planetary geostrophic ocean circulation model (ZLG, ZGL). Unlike more sophisticated coupled ice-ocean models, we focus on the effects of sea-ice on the stability and variability of the thermohaline circulation, instead of the influence of the ocean on the ice. Idealized annual mean surface temperature and salinity forcings are used, together with an idealized flat-bottomed box ocean basin of 60° extent in both latitude and longitude, from 5 N to 65 N and of 4 km depth. The horizontal resolution used is 2° in both latitude and longitude, with 14 vertical levels.

The coupled ice-ocean model is first spun up using restoring conditions on the surface salinity and temperature. The equivalent atmospheric temperature is lowered at the high latitudes compared to ZGL so that ice is simulated in this control run. We then switch to mixed conditions, where the salinity flux is diagnosed from the control simulation and is specified as a surface forcing. The results show an oscillation in various model parameters with a period of 17 years. The thermal insulation of an ice cover is the primary mechanism responsible for this variability. As ice only develops in regions where there is heat loss to the atmosphere, an increasing ice cover means that the ocean basin will gain heat and hence warms up. This heat is carried northward by the thermohaline circulation where it melts the ice and reduces the ice cover. The enhanced surface heat loss over open water then leads to ice formation and an oscillation ensues. For this oscillation, obtained using a restoring condition for the surface temperature and annual mean forcing, salinity rejection is of secondary importance compared to the thermal insulating role of the ice cover. This was shown by repeating the model experiment with the salinity rejection/dilution effect removed. To understand this, we noted that as ice starts to form or grow, the flux of heat through the ice is reduced by the insulating effect. The convective flux of heat from the deep ocean must then reduce even more in order to meet the ice growing condition that there be a divergence of the heat flux at the base of the ice; i.e. that the $F_i - F_o$ term in Eq. (1) be negative. For this to happen, the surface model level must become less dense, showing that salinity rejection can, at best, play only a secondary role in modifying surface density. In fact, we showed in Section 5 that changes in surface salinity are dominated by the change in the

convective flux of salt into the surface level from below. The analysis in Section 5 also showed that including seasonal forcing could considerably enhance the importance of salinity rejection. Preliminary results using seasonal forcing to drive our model confirm the importance of salinity rejection on the seasonal time scale. However, superimposed on the seasonal cycle is an interdecadal oscillation such as described in this paper.

The association of low surface salinities with increased amounts of sea-ice, such as found in our model, has been noted by Marsden *et al.* (1991). The stabilizing effect of low surface salinity for the development of sea-ice anomalies is a feature of the interdecadal oscillation mechanism proposed by Mysak *et al.* (1990). The presence of the Great Salinity Anomaly in the Labrador Sea, with its associated fresh water cap, is known to have inhibited the formation of Labrador Sea Water in the late 1960's and early 1970's (Lazier, 1980), at a time of greater than normal ice extent (Manak and Mysak, 1989). Deser and Blackmon (1993) have also noted a two year lag between increased ice extent in the Labrador Sea and lower than normal SST to the east of Newfoundland, with the ice extent leading. These authors identified two distinct modes of SST variability in the North Atlantic. The first is associated with the gradual warming during the 1920's and 30's followed by a cooling during the 1960's. The second also exhibits decadal time scale variability and is the one associated with the ice extent in the Labrador Sea. We suggest our model may be of some relevance for explaining this mode.

Through a conceptual model, we have determined that the simulated time scale of 17 years depends on the effective rate of heat transfer from the open ocean to the layer under the ice. Changing the restoring time scale for the surface temperature from 30 days to 50 days increases the oscillation period to near 30 years. The conceptual model also predicts a phase difference of 90° between the ice cover and basin mean temperature; the simulated phase difference is 45°. This discrepancy probably reflects the role played by the thermohaline circulation in transporting heat poleward.

Our results show the importance to ocean-climate interaction of the thermal feedback associated with an ice cover. The results also suggest a mechanism for decadal variability in the ocean which depends on the ice-ocean interaction. This is different from the advective mechanism of Weaver and Sarachik (1991a). It is also a different mechanism from that driving the interdecadal oscillations under constant heat flux found by Greatbatch and Zhang (1994).

A question remains as to the influence played by the simple treatment we have adopted for the surface freshwater flux. This allows the freshwater flux diagnosed from the restoring spin-up to pass through the ice, except for that part used for snow accumulation. It is then modified by salinity rejection/dilution due to ice formation/melting. It is this diagnosed freshwater flux that provides the source of freshwater leading to the high correlation between low surface salinity and enhanced ice extent

in our results. The mechanism is similar to that of the polar halocline catastrophe discussed by ZGL and arises because of the reduced surface heat flux arising from the insulating effect of the ice cover. A high correlation between low surface salinity and enhanced ice extent is also a feature of observed data (Marsden *et al.,* 1991). A possible interpretation is that the freshwater flux in our model is due to run-off. However, we admit our treatment of the surface freshwater flux is very simple. Future work will address the question of how to improve this aspect.

Acknowledgments. This work forms part of the Canadian university participation in the World Ocean Circulation Experiment (WOCE), and is supported by Collaborative Research Initiative Program of the Natural Sciences and Engineering Research Council (NSERC) of Canada. We are grateful to Ursula Seidenfuss for drafting help with the figures.

REFERENCES

Bjerknes, J. 1964. Atlantic air-sea interaction. Adv. Geophys, *10,* 1–82.

Bryan, F. 1986a. Maintenance and variability of the thermohaline circulation. Ph.D thesis, Atmospheric and Oceanic Sciences Program, Princeton University, U.S.A.

—— 1986b. High-latitude salinity effects and interhemispheric thermohaline circulations. Nature, *323,* 301–304.

Bryan, K. 1969. A numerical method for the study of the circulation of the world ocean. J. Comput. Phys., *4,* 347–376.

Bryan, K. and M. D. Cox. 1972. An approximate equation of state for numerical models of the ocean circulation. J. Phys. Oceanogr., *2,* 510–514.

Bryan, K. and R. J. Stouffer. 1991. A note on Bjerknes' hypothesis for North Atlantic variability. J. Mar. Res., *1,* 229–241.

Cox, M. D. 1984. A primitive equation, 3-dimensional model of the ocean. GFDL Ocean Group Technical Report No. 1, GFDL/Princeton University, U.S.A.

Delworth, T., S. Manabe and R. J. Stouffer. 1993. Interdecadal variations of the thermohaline circulation in a coupled ocean-atmosphere model. J. Climate, *6,* 1993–2011.

Deser, C. and M. L. Blackmon. 1993. Surface climate variations over the North Atlantic Ocean during winter: 1900–1989. J. Climate, *6,* 1743–1753.

Dickson, R. R., J. Meinke, S.-A. Malmberg and A. J. Lee. 1988. The great salinity anomaly in the northern North Atlantic, 1968–1982. Prog. Oceanogr., *20,* 103–151.

Gordon, A. L., S. E. Zebiak and K. Bryan. 1992. Climate variability and the Atlantic Ocean. EOS, *73,* 161–165.

Greatbatch, R. J. and S. Zhang. 1994. An interdecadal oscillation in an idealized ocean basin forced by constant heat flux. J. Climate, (in press).

Hakkinen, S. 1993. An Arctic source for the Great Salinity Anomaly: A simulation of the Arctic ice-ocean system for 1955–75. J. Geophys. Res., *98*(C9), 16, 397–16, 410.

Hakkinen, S. and G. L. Mellor. 1992. Modeling the seasonal variability of a coupled Arctic ice-ocean system. J. Geophys. Res., *97*(C12), 20, 285–20, 304.

Haney, R. L. 1971. Surface thermal boundary condition for ocean circulation models. J. Phys. Oceanogr., *1,* 241–248.

Hibler III, W. D. 1979. A dynamic-thermodynamic sea ice model. J. Phys. Oceanogr. *9,* 815–846.

—— 1980. Modelling a variable thickness sea ice cover. Mon. Wea. Rev., *108,* 1943–1973.

Hibler, III W. D. and K. Bryan. 1987. A diagnostic ice-ocean model. J. Phys. Oceanogr., *17,* 987–1015.

Huang, R. X. and L. Chou. 1994. Parameter sensitivity study of the saline circulation. Climate Dynamics, *9,* 391–409.

Kushnir, Y. 1994. Interdecadal variations in North Atlantic sea surface temperature and associated atmospheric conditions. J. Climate, *7,* 141–157.

Lazier, J. R. N. 1980. Oceanographic conditions at Ocean Weather Ship Bravo, 1964–1974. Atmosphere-Ocean *18,* 227–238.

Manak, D. K. and L. A. Mysak. 1989. On the relationship between Arctic sea ice anomalies and fluctuations in Northern Canadian air temperature and river discharge. Atmosphere-Ocean, *27,* 682–691.

Marotzke, J., P. Welander and J. Willebrand. 1988. Instability and multiple steady states in a meridional-plane model of thermohaline circulation. Tellus, *40A,* 162–172.

Marsden, R. F., L. A. Mysak and R. A. Myers. 1991. Evidence for stability enhancement of sea ice in the Greenland and Labrador sea. J. Geophy. Res., *96,* 4783–4789.

Maykut, G. A. and N. Untersteiner. 1971. Some results from a time dependent thermodynamic model of sea-ice. J. Geophys. Res., *76,* 1550–1575.

Mysak, L. A. and C. A. Lin. 1990. Role of the oceans in climatic variability and climate change. Can. Geographer., *34,* 352–369.

Mysak, L. A., D. K. Manak and R. F. Marsden. 1990. Sea-ice anomalies observed in the Greenland and Labrador Seas during 1901–1984 and their relation to an interdecadal Arctic climate cycle. Clim. Dyn., *5,* 111–133.

Mysak, L. A. and S. B. Power. 1992. Sea-ice anomalies in the western Arctic and Greenland-Iceland Sea and their relation to an interdecadal climate cycle. Clim. Bull., *26,* 147–176.

Roed, L. P. 1984. A thermodynamic ice ocean model of the marginal ice zone. J. Phys. Oceanogr., *14,* 1921–1929.

Saltzman, B. 1978. A survey of statistical-dynamical models of the terrestrial climate. Advances in Geophysics, *20,* 183–304.

—— 1982. Stochastically-driven climatic fluctuations in the sea-ice, ocean temperature, CO_2 feedback system. Tellus, *34,* 97–112.

Saltzman, B. and R. E. Moritz. 1980. A time-dependent climatic feedback system involving sea-ice extent, ocean temperature, and CO_2. Tellus, *32,* 93–118.

Saltzman, B., A. Sutera and A. Evenson. 1981. Structural stochastic stability of a simple auto-oscillatory climatic feedback system. J. Atmos. Sci., *38,* 494–503.

Semtner, A. J. 1976. A model for the thermodynamic growth of sea ice in numerical investigations of the climate. J. Phys. Oceanogr., *6,* 379–389.

—— 1987. A numerical study of sea ice and ocean circulation in the Arctic. J. Phys. Oceanogr., *17,* 1077–1099.

Weaver, A. J. and T. M. C. Hughes. 1992. Stability and variability of the thermohaline circulation and its link to climate. Report No. 92-5, Centre for Climate and Global Change Research (C^2GCR), McGill University, Canada, 56 pp.

Weaver, A. J. and E. S. Sarachik. 1991a. Evidence for decadal variability in an ocean general circulation model: An advective mechanism. Atmosphere-Ocean, *29,* 197–231.

——, 1991b. The role of mixed boundary conditions in numerical models of the ocean's climate. J. Phys. Oceanogr., *21,* 1470–1493.

Weaver, A. J., E. S. Sarachik and J. Marotzke. 1991. Fresh water flux forcing of decadal and interdecadal oceanic variability. Nature, *353,* 836–838.

Welander, P. 1977. Thermal oscillations in a fluid heated from below and cooled to freezing from above. Dyn. Atmos. Oceans., *1,* 215–223.

Yang, J. and J. D. Neelin. 1993. Sea-ice interaction with the thermohaline circulation. Geophys. Res. Lett., *20,* 217–220.

Zhang, S., R. J. Greatbatch and C. A. Lin. 1993. A re-examination of the polar halocline catastrophe and implications for coupled ocean-atmosphere modelling. J. Phys. Oceanogr., *23,* 287–299.

Zhang, S., C. A. Lin and R. J. Greatbatch. 1992. A thermocline model for ocean climate studies. J. Mar. Res., *50,* 99–124.

Received: *30 March, 1993;* revised: *13 October, 1994.*